M.M. Sarafraz, M. Jafarian, M. Arjomandi, G.J. Nathan

Potential use of liquid metal oxides for chemical looping gasification: a thermodynamic assessment

Applied Energy, 2017; 195:702-712

Potential use of liquid metal oxides for chemical looping gasification: A thermodynamic assessment

M. M. Sarafraz[1,*], M. Jafarian[1], M. Arjomandi[1], G. J. Nathan[1]

[1]Centre for Energy Technology, School of Mechanical Engineering, University of Adelaide, SA 5005, Australia.

[*corresponding author]

Email: mohammadmohsen.sarafraz@adelaide.edu.au

Tel: +61416311335

Abstract:

A new concept for syngas production is proposed in which a liquid metal oxide (here copper oxide) is implemented as an oxygen carrier for chemical looping gasification. The proposed system consists of two interconnected bubble reactors as the fuel and air reactors, through which a liquid metal oxide is circulated to be successively reduced and oxidised providing the required heat and oxygen for the gasification reaction. The proposed system offers a potential process to avoid challenges such as agglomeration and sintering that are typically associated with the solid metal oxides that have previously been proposed for chemical looping gasification. Thermochemical equilibrium models are presented that show acceptable agreement with the available data. The model is then used to estimate that the carbon conversion of feedstock is up to 84.6% for gasification and 100% for combustion with the proposed concept. In addition, the mole fraction of gaseous copper oxide in the outlet stream from the air reactor is estimated to be 10^{-11}, which implies that no further process is required to separate the evaporated copper oxide from the syngas.

Keywords: thermochemical cycle; chemical looping gasification; liquid copper oxide; syngas production; sensitivity analysis

1. Introduction

Chemical Looping Gasification (CLG) is a recently developed process with a potential to avoid the dilution of the syngas with N_2 by producing the oxygen from reduction-oxidation (Red-Ox) reactions [1-3]. In CLG, an oxygen carrier (OC), typically a metal oxide in the form of solid particles is employed to partially oxidise the fuel in one reactor, referred to as the fuel reactor, thus avoiding the direct contact between the fuel and nitrogen from the air. The reduced OC particles are then oxidised in another reactor, referred to as the air reactor. The system typically is configured to supply the heat required in the fuel reactor from that released in the air reactor. Loop seals are usually employed between the two reactors to mitigate gas leakage between them during the cycling of the OC particles [4]. Notwithstanding the advantages of the solid OC particles, they also introduce some challenges to the system. These include not only agglomeration and sintering [5-14], but also the need to separate the OC particles from any carry-over particles from the gasifier and also that to manage the deposition of carbon and ash onto the OC particles, which tends to block their pores [15]. These challenges significantly reduce the effectiveness of the OC particles in transporting oxygen between the reactors [14, 16-20], which decreases the efficiency of the process [5]. For example, the gasification of biomass using CLG reported by Acharya et al. [17] only achieved 40% regeneration of the CaO solid particles at a calcination temperature of 800°. A low regeneration efficiency of 50% was also reported by Li et al. [21] with similar values reported elsewhere [5, 16, 22-25]. Hence, although investigations are in progress to seek suitable techniques to mitigate these disadvantages [5-14], it is desirable to identify alternative chemical looping gasification concepts that potentially can bypass them altogether.

The use of a liquid metal oxide as the oxygen carrier for CLG is a potential approach to address the technical challenges associated with the use of solid OC particles. Although it may bring some new challenges. Application of molten metals is a well-known process used for gasifying a carbonaceous feedstock in a heat recovery unit from metal-containing slag at high temperature conditions [26, 27]. Molten slag is a mixture of metal oxides and organic materials such as SiO_2, Al_2O_3, CaO, FeO and MgO and is a by-product of ironmaking process in a blast furnace [28]. Molten slag leaves a blast furnace at a temperature of up to 1650 °C, hence, its sensible heat can be employed to drive a downstream gasification reaction. In this process, the carbonaceous fuel is partially (or totally) oxidized, typically in the presence of a gasifying agent such as steam and/or CO_2, by injecting it into a high temperature molten slag. Nevertheless,

while it is well known that slags have potential to act as a gasifying medium, no systematic investigation of pure liquid metal oxides and their thermodynamic potential for chemical looping gasification is available.

The process of gasification of carbonaceous feedstock such as coal in molten slag with either steam and/or CO_2 as the gasifying agent has been found to offer some significant advantages and disadvantages over conventional processes. In particular, it offers high rates of heat and mass transfer, which results in good controllability in operation and syngas quality. Hence, the ratio of the H_2/CO can be readily adjusted through the ratio of CO_2/feedstock or H_2O/feedstock, which leads to the high carbon conversion rates and high quality of the syngas product [29-35]. Nevertheless, the use of slags for gasification has been found to suffer from the disadvantage of a low thermal conductivity (1 W/m.K for slag versus 120W/m.K for molten copper oxide [36], respectively) due to the presence of minerals. In addition, slag tends to form layers of fused materials of different compositions (e.g. silica layer, minerals and non-metallic compounds,) with relatively low thermal conductivity, which deteriorate the thermal performance of the process [26, 27]. However, little attention has been paid to the use of molten metal oxides, which have the potential to retain the good heat transfer characteristics. One aim of the present investigation is therefore to explore this gap.

It has also been shown that molten metals can enhance the rate of reaction because they induce a catalytic effect to the gasification reactions [37-39]. This suggests that it may be possible to achieve relatively low-temperature gasification process if the right type of metal can be identified, which would offer the potential for a low-cost process. However, to date no systematic investigation of the potential of different metal/metal oxides has been undertaken to seek to identify metals that could exploit this potential. The present investigation therefore aims to meet this need.

The potential to harness the properties of molten metal oxides as an oxygen carrier in a chemical looping process was recently proposed by Jafarian et al. [4], to reform natural gas using iron/iron oxide. Their proposed system comprises two inter-connected bubbling column reactors to circulate the liquid between the air and fuel reactors. Their thermodynamic analysis shows that the conversion of the natural gas to CO_2 and H_2O depends strongly on the flow rate of circulating liquid oxygen carrier (LOC) between the air and fuel reactors. That is, a higher circulation flow rate of LOC between the reactors than stoichiometric value is required for the complete conversion of the fuel to H_2O and CO_2, while a lower circulation flow rate than

stoichiometric value results in carbon monoxide production. However, no similar assessment of the potential of other metals or fuels has yet been performed.

In the light of above discussion, the primary objective of the present work is to investigate the thermodynamic feasibility of the concept of Liquid Chemical Looping Gasification (LCLG) for the partial oxidation of the fuel to produce syngas. We further aim to assess the influence of different operating parameters on the quality and quantity of syngas production. Finally, we also aim to assess the potential to implement the chemical path, although the detailed assessment of the technical feasibility of this system is well beyond the scope of the present investigation.

2. Thermodynamics of liquid copper oxide in the LCLG

2.1.Phase diagram

Figure 1 represents the phase diagram of copper and oxygen as a function of temperature and partial pressure of the dissolved oxygen. In the region above the line A-B-C-D-E, a homogenous liquid slag is formed with a variable mole fraction of oxygen, spanning the range from ~0.01 (at point A) to ~0.5 (at point D). Below this line, the slag comprises both the solid and liquid phases with known composition of copper and oxygen in a two-phase mixture. This regime is inappropriate for the LCLG system because of the technical challenges of operating the reactors in a two-phase regime. In addition, the complex heat and mass transfer between the phases is difficult to predict. In contrast, the region above the line A-B-C-D-E is technically and thermodynamically preferred for the LCLG process. Therefore, LCLG regime is assessed in this region.

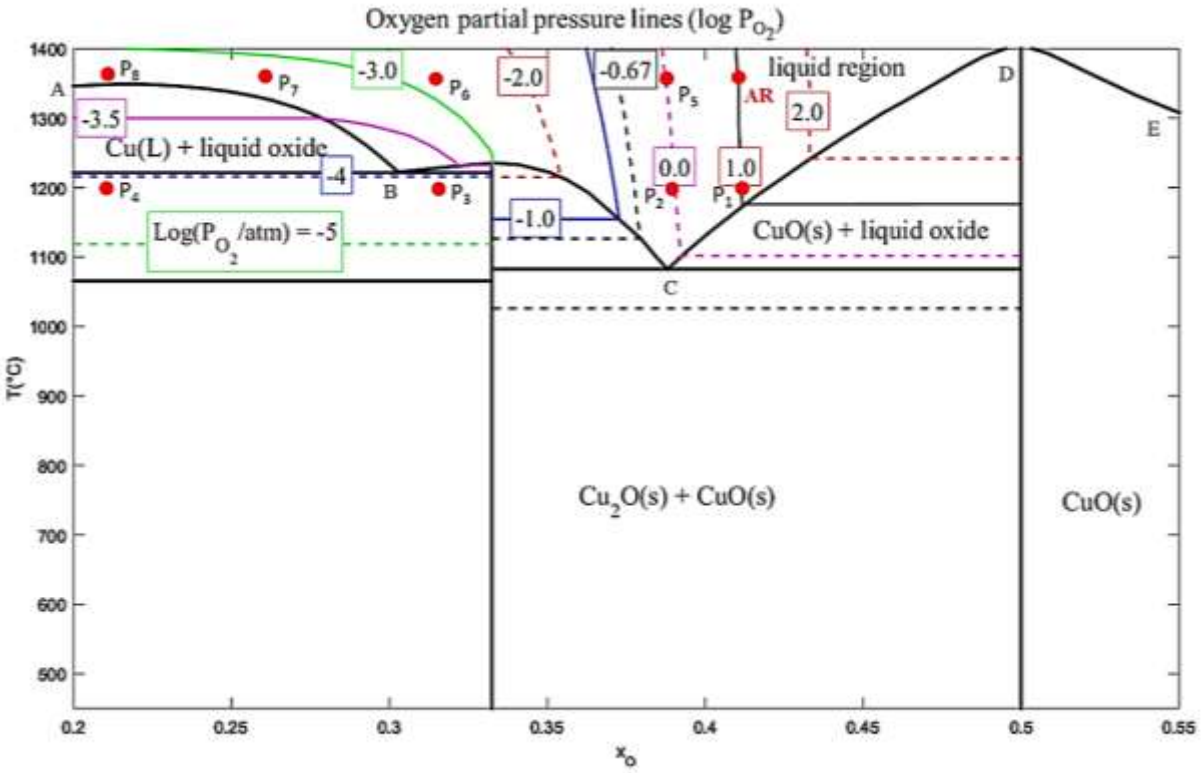

Fig. 1. Phase diagram for Cu-O system, adapted from elsewhere [40, 41]. The homogenous molten metal oxide above line A-B-C-D-E is considered the most suitable region for the gasification process. AR is a typical condition for the air reactor. While P_5 to P_8 are possible conditions for the fuel reactor.

2.2.Assumptions

The simulation and model used here rely on the following assumptions:

1. The reactions are at an equilibrium.
2. Heat losses from the fuel and air reactors are neglected.
3. A system is available to transfer the LOC between air and fuel reactors fluid-mechanically) with negligible energy requirement.
4. No solidification occurs in the system and conditions are sufficiently far from any solid-liquid two-phase regions.
5. Any impurities in the fuel have a negligible influence on the reactions and only carbon reacts in the gasifier.
6. An ash separator is available to completely separate the ash from the LOC.
7. The residence time is sufficient for the reactions to reach completion so that no carbon enters the air reactor.

8. Heat loss is negligible from all pipes, tanks and units.
9. The total exergy of the fuel is equivalent to that of syngas product and that carried by the vitiated air.

2.3.HSC and R-Gibbs aspen plus models

Graphite was selected as a surrogate for the carbonaceous fuel here. This is because carbon is the primary component of coal and biomass, while being simpler to analyse. As can be seen from the phase diagram (shown in Figure 1), the $CuO_{\delta}(l)$, above the line A-b-C-D-E, comprises a mixture of Cu (l), Cu_2O (l) and/or CuO (l), depending on the mole fraction of oxygen in the system. Therefore, these components are selected for the liquid phase reactions. The reducing agents considered are C, H_2, CO and CH_4. The three gaseous species can be produced through reactions such as methane reforming, the Boudouard reaction and the water-gas shift reaction. Furthermore, CO can also be produced through incomplete oxidation of C with molten copper oxide, while H_2 can be also produced through reduction of water by the molten copper oxide. The selection of these components was then cross-checked using HSC Chemistry software at the relevant conditions. This revealed that the concentration of other hydrocarbons is of the order of 10^{-6}, which justifies neglecting them.

In the absence of kinetic data of the gasification with copper oxide, thermodynamic assessments have been undertaken to identify plausible chemical pathways. It is assumed that the molten phase of copper oxide (shown as $CuO(\delta)$) comprises the components of CuO (l), Cu_2O (l) and pure Cu (l), which react with the graphite in accordance with equations 1 and 2. In the next step, molten copper is assumed to react with the carbon monoxide product in accordance with equations 3 and 4. The reaction of graphite with steam forms methane (equation 10), which reacts with the molten copper according to equations 5 and 6. Importantly, the Gibbs free energy for the reaction between CuO and steam is positive so that it will not proceed (equations 7 and 8). Instead, the Boudouard reaction, water-gas and water-gas shift reactions, shown in from equations 10-12, occur simultaneously with the other reactions in the fuel reactor. Likewise, equations 13 and 14 occur in the air reactor, where molten copper reacts with the oxygen in the air to complete the Red-Ox thermochemical cycle. That is four groups of reactions occur in the different stages of the process.

2.3.1. Reduction reactor

- **Reactions between liquid and solid phases [42]**

$$2CuO(l) + C(s) \rightarrow Cu_2O(l) + CO(g), \quad (1)$$

$$Cu_2O(l) + C(s) \rightarrow 2Cu(l) + CO(g), \quad (2)$$

- **Reactions between liquid and gas phases [43, 44]**

$$2CuO(l) + CO(g) \rightarrow Cu_2O(l) + CO_2(g), \quad (3)$$

$$Cu_2O(l) + CO(g) \rightarrow 2Cu(l) + CO_2(g), \quad (4)$$

$$CH_4(g) + 2CuO(l) \rightarrow 2H_2(g) + CO(g) + Cu_2O(l), \quad (5)$$

$$CH_4(g) + Cu_2O(l) \rightarrow 2H_2(g) + CO(g) + 2Cu(l), \quad (6)$$

$$2Cu(l) + H_2O(g) \rightarrow Cu_2O(l) + H_2(g), \quad (7)$$

$$Cu_2O(l) + H_2O(g) \rightarrow 2CuO(l) + H_2(g), \quad (8)$$

- **Reactions between solid and gas phases**

Methane formation [45, 46]

$$C(s) + 2H_2(g) \rightarrow CH_4(g), \quad (9)$$

Primary water gas reaction [47]

$$C(s) + H_2O(g) \rightarrow CO(g) + H_2(g), \quad (10)$$

Boudouard reaction [48, 49]

$$C(s) + O_2(g) \rightarrow 2CO(g), \quad (11)$$

- Reactions within gas phase

Water-gas shift reaction [50]

$$CO(g) + H_2O(g) \rightarrow CO_2(g) + H_2(g), \quad (12)$$

Oxidation reactor

- **Reactions between liquid and gas phases**

$$Cu_2O(l) + O_2(g) \rightarrow CuO(l), \quad (13)$$

$$Cu(l) + O_2(g) \rightarrow Cu_2O(l), \quad (14)$$

To assess the aforementioned reactions, thermochemical equilibrium analysis and Gibbs minimization methods are applied using HSC chemistry software. The model was solved for 1 kmol for each of the reactants graphite and steam under the reference condition described in Table 1. A sensitivity analysis was then performed for different operating temperatures and pressures and the ratio of the flow rates of LOC and steam to fuel, which are defined in section 4.

3. Concept of Liquid Chemical Looping Gasification (LCLG)

Figure 2 presents a schematic diagram of the Liquid Chemical Looping Gasification (LCLG) process assessed here. A plausible configuration with which to implement the process comprises two interconnected bubble reactors proposed by Jafarian et al. [4]. The fuel reactor is proposed to reduce the LOC and produce syngas, while the air reactor is proposed to oxidise the LOC and produce high temperature vitiated air. The bubbling medium is chosen because such systems are known to generate high rates of heat and mass transfer and can also generate circulation via the density difference between two reactors [51-57].

A disk separator utilising the density difference between the ash and slag [58, 59] has been identified as a plausible means for this process [4]. However, further work is required to evaluate the technical and economic feasibility of this or other devices.

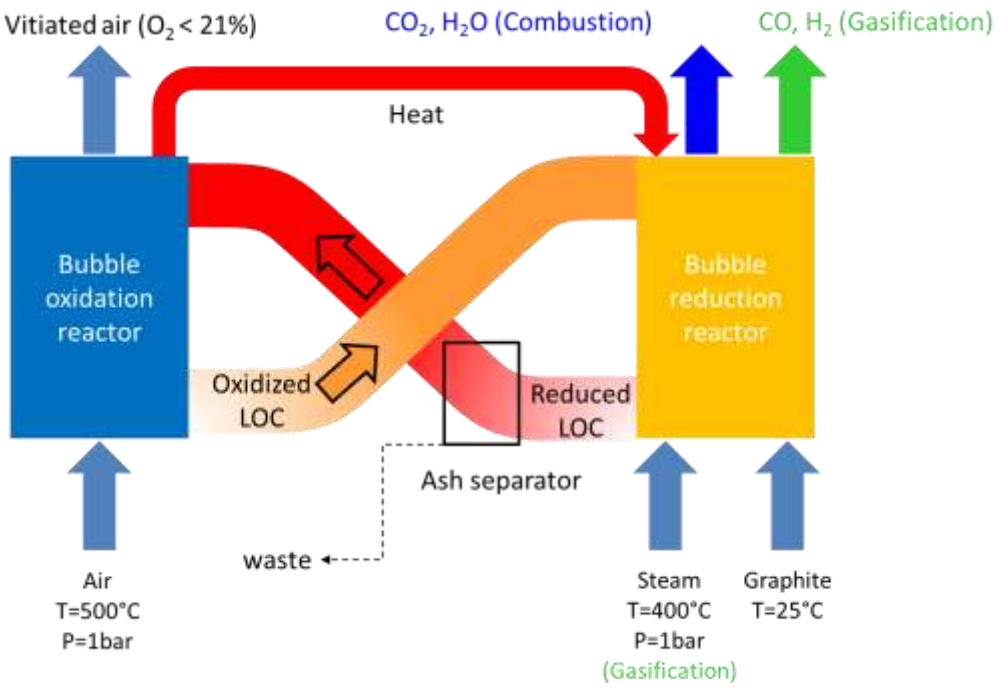

Fig. 2. A schematic diagram of the proposed LCLG configuration.

4. Methodology

The enthalpy of reaction as a function of temperature was estimated using HSC chemistry software based on the phase diagram of the copper-oxygen binary system and the results were compared with data from the literature [40, 41]. Thermochemical equilibrium analysis was used to simulate the gasification process. Two additional equations were used to relate the fraction of oxygen in the liquid copper oxide (x_O) to the composition of liquid copper oxide [42] as follows:

$$n_{CuO} = \frac{3x_o - 1}{1 - x_o}, \tag{15}$$

And

$$n_{Cu_2O} = \frac{1 - 2x_o}{1 - x_o}, \tag{16}$$

The fraction of exergy of the syngas product to that of the inlet fuel $\chi_{Ex,syngas-fuel}$ is defined as follows:

$$\chi_{Ex,syngas-fuel} = \left. \frac{\sum_{i=1}^{n} n_{syngas} . LHV_{syngas}}{n_{graphite} . LHV_{graphite}} \right|_{products} . \tag{17}$$

Equation 17 was used to compare the fraction of exergy in the syngas product with that of the original fuel, where n_i is the mole fraction of the products and LHV is the Lower Heating Value of the syngas and fuel. The ratio of the flow rates of LOC and steam to fuel were defined to investigate their influence on the gasification performance [18] as follows:

$$\varphi = \frac{\dot{n}_{LOC}}{\dot{n}_{fuel}}, \tag{18}$$

$$\psi = \frac{\dot{n}_{steam}}{\dot{n}_{fuel}} . \tag{19}$$

Table 1 presents the main operating conditions considered with the model.

Table 1. Reference operating conditions for the reduction and oxidation reactors.

Unit	Air	Fuel	Steam	LOC (mole)			T(°C)	P(bar)
	(kmol)	(kmol)	(kmol)	Cu(l)	CuO(l)	Cu_2O(l)		
Air reactor	1	-	-	-	0.508	0.245	1300	10
Fuel reactor	-	1	1	0.05		0.21	1300	10

A sensitivity analysis was employed to assess the influence of φ and ψ on the quality and quantity of the syngas relative to a reference point defined in Table 1. The influence of φ and ψ on the fuel conversion is also assessed using equation 20 [18, 60] as follows:

$$X_c = \frac{n_{Fuel,init} - n_{Fuel,cons}}{n_{Fuel,init}}. \quad (20)$$

The flow rate of air, $\dot{n}_{air}$ relative to that of the LOC within the oxidation reactor was also defined as follows:

$$\lambda_O = \frac{\dot{n}_{air}}{\dot{n}_{LOC}}. \quad (21)$$

This parameter characterises the performance of the oxidation reactor and also determines the rate of regeneration of the LOC in the air reactor.

5. Verification of the results

To partially validate the model, the results obtained for the gas production and syngas quality were compared with previous studies on gasification with molten slag reported by Yu et al. [61]. To the best of our knowledge, neither theoretical nor experimental investigations of gasification using molten metal have been reported previously. Figure 3 presents the syngas quality (H_2/CO) estimated with the HSC model in comparison with Yu et al. [61] for two different steam to fuel ratios at 1200°C. As can be seen, the results calculated for syngas quality agree with those of calculated by Yu et al. [61] to within an absolute average deviation of ±16%. This is deemed to be sufficiently reliable for the present assessment of thermodynamic feasibility of the system.

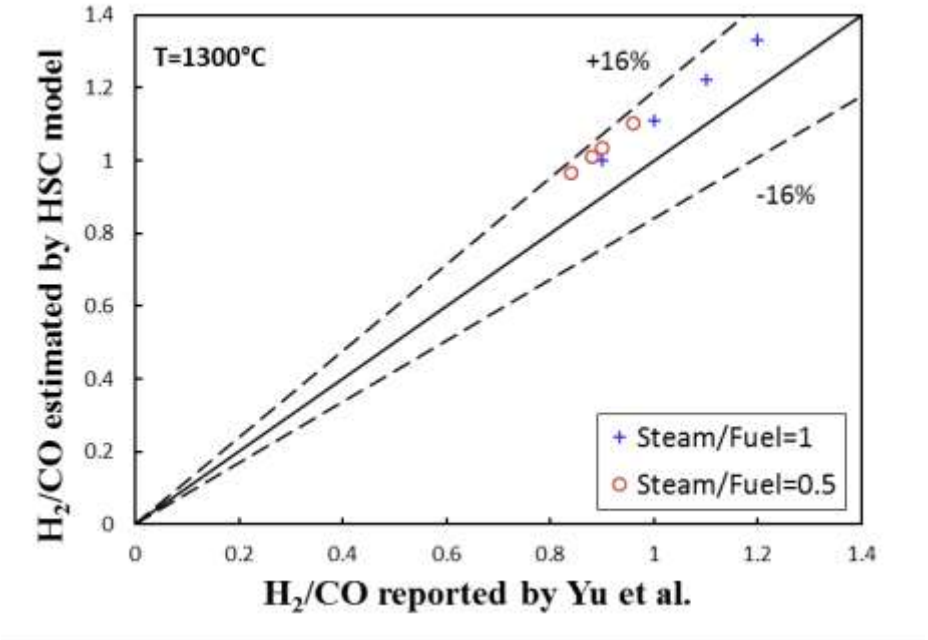

Fig. 3. Comparison between H_2/CO obtained by the HSC model and those of reported in the literature [49].

6. Results and discussion

6.1.Gibbs free energy of the reactions

Figure 4 presents the calculated values of the Gibbs free energy for the reduction reactions as a function of temperature, as simulated with HSC chemistry, referred to as an Ellingham diagram. This shows that the value of the Gibbs free energy is negative for all reactions in the gasifier at temperatures ranging from 1200°C -1500°C, implying that the reactions in liquid-gas phases, specifically between CuO (l) and Cu_2O(l) with the fuel, gasifying agent and other compounds are spontaneous.

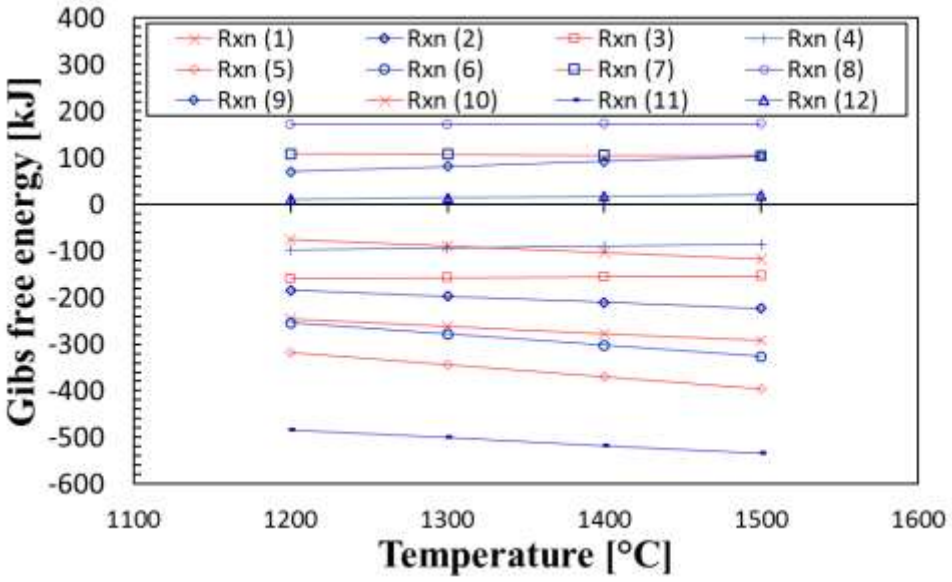

Fig. 4. Dependence of Gibbs free energy for the reduction reactions of liquid copper oxide on temperature.

Figure 5 presents the calculated values of the Gibbs free energy for the oxidation reactions as a function of temperature. As can be seen, the values of the Gibbs free energy for the oxidation reactions are also negative so that the reactions are also spontaneous. Furthermore, the calculated Gibbs free energy decreases linearly with an increase in the operating temperature of the reactor.

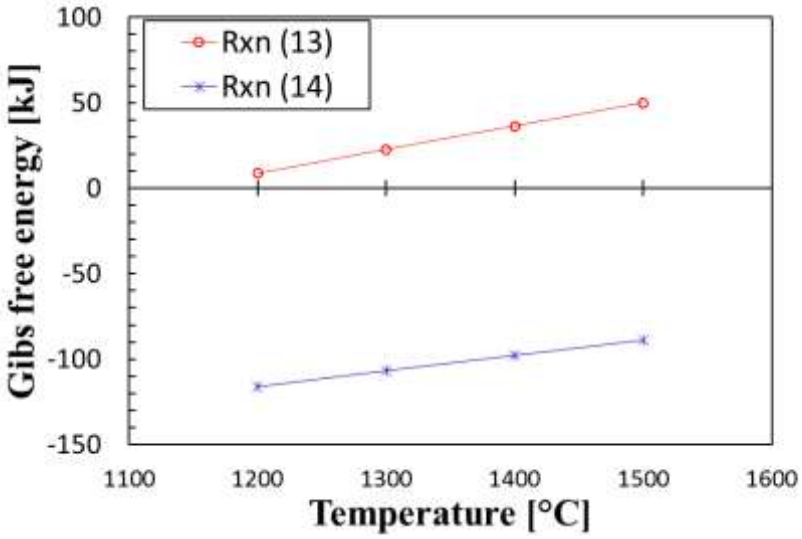

Fig.5. Dependence of Gibbs free energy on temperature for oxidation reactions of liquid copper oxide.

Figure 6 presents the calculated dependence of the enthalpy of reactions on temperature for the reduction and oxidation reactions together, some of which are exothermic (e. g. the water-gas shift reaction and the catalytic copper oxide reactions with graphite), and some of which are endothermic (e. g. the main Boudouard gasification reaction). The net enthalpy of the reactions in the gasifier and oxidation reactors are endothermic and exothermic, respectively. However, the heat released in the oxidation reactor is sufficient to supply the heat that required for the fuel reactor. Thus, it is thermodynamically possible to avoid the need for any external energy sources to maintain the required heat, provided that the energy is transferred effectively and that the heat losses are sufficiently small.

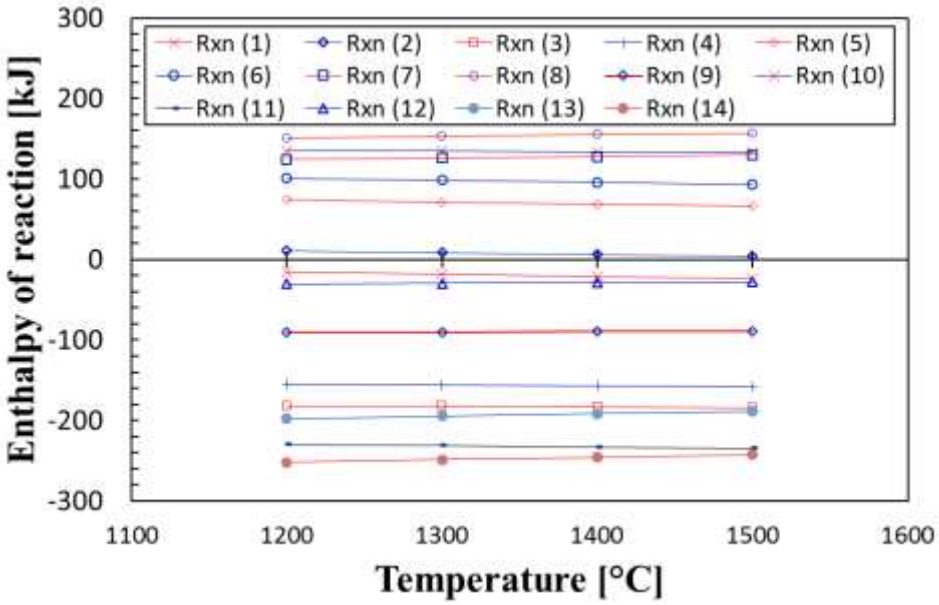

Fig. 6. Dependence of the enthalpy of reaction on temperature for different gasification reactions using liquid copper oxide.

6.2. Assessment of fuel reactor for the syngas production

Figure 7 presents the dependence on φ of carbon dioxide production with the proposed system for two different operating temperatures of the fuel reactor, namely at 1200°C and 1350°C. As shown in Fig. 7, for LOC circulation ratios of less than 8, the oxygen ratio in the fuel reactor is sub-stoichiometric and the proposed system operates in the gasification regime. In this condition, partial oxidation of graphite produces mostly CO instead of CO_2. The presence of steam as the gasifying agent provides the hydrogen for the syngas product. With an increase in the circulation ratio, the stoichiometric ratio increases and the reactions proceed towards complete combustion.

Returning to Fig. 1, we consider four different operating points for each of two given temperatures (P_1-P_4 for 1200°C and P_5-P_8 for 1350°C). As can be seen, at 1200°C, the fuel reactor would need to operate in the two-phase regime at low values of φ, which is technically challenging for bubble column reactors. However, at an operating temperature of 1350°C, the conditions in the fuel reactor are only in the liquid phase for all values of φ, which is necessary to enable circulation. Nevertheless, operation at this high-temperature condition is challenging.

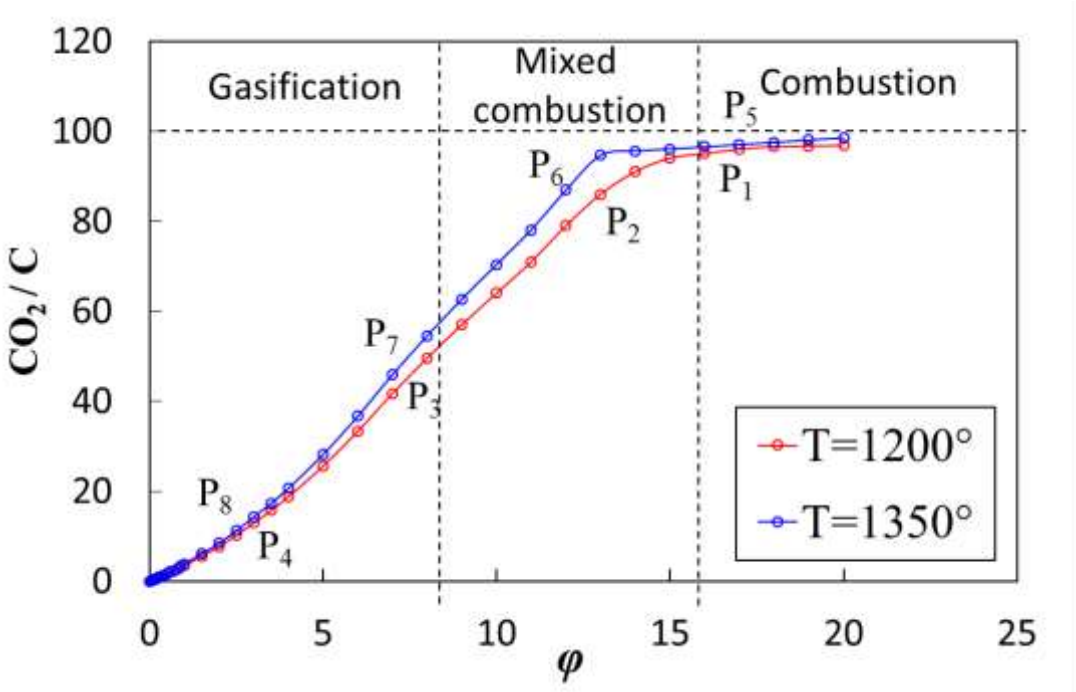

Fig. 7. Dependence on φ of CO_2/C for different temperatures of 1200°C and 1350°C.

Figure 8 presents the dependence of CO_2/CO on φ. As can be seen, three distinguishable regimes can be seen, namely the gasification, mixed combustion and total combustion regimes. In the gasification regime, ($0 < \varphi < 8$), the quality of syngas varies from 0.92 to 2.9, while for mixed combustion it is less than 1.32. In addition, CO production from the gasification regime changes slightly with the circulation ratio. However, due to the production of CO_2 in regime 2, the value of CO_2/CO changes considerably. For example, CO_2/CO=4 for φ=9, while it reaches 40 for φ=16. This reveals that in regime 2, due to the carbon dioxide production, the system works partly in the gasification and partly in the combustion regimes. Therefore, the final product in the mixed combustion regime is CO, H_2 and CO_2. For the total combustion regime, the main products are heat and carbon dioxide, which can be stored and sequestrated. Therefore, regime I is appropriate for producing the high-quality syngas. It is noteworthy

saying that the quality of syngas can be controlled by φ and ψ, which is discussed in more details below.

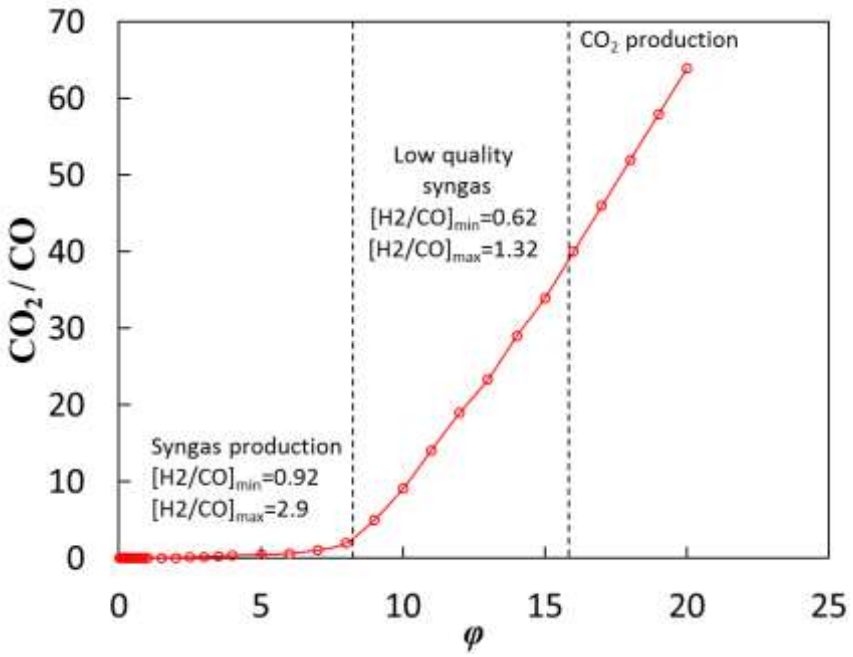

Fig. 8. Dependence on φ of CO_2/CO at T=1350°C and for ψ=1.

6.3.Influence of temperature on the syngas quality for different φ

Figure 9 presents the dependence of syngas quality (H_2/CO) on temperature for different values of φ. Here, syngas is defined based on its application for a Fischer-Tropsch, (F-T) process, for which the desirable H_2/CO ratio is greater than or equal to 2 [62]. It can be seen that the H_2/CO decreases weakly with an increase in T and strongly with an increase in φ. For instance, H_2/CO=1 for φ =0.01, ψ=1 and T=1200°C. However, for φ =5, and other conditions being the same, the syngas quality is 0.5. The decrease in H_2/CO with an increase in operating temperature is due to the increase in production of CO. An increase in temperature from 1200°C to 1400°C decreases the syngas quality from 0.9 to 0.86. It can also be seen that a value of H_2/CO=2 can be achieved for sufficiently low φ in the range of 0.01-0.1 and for specific values of ψ.

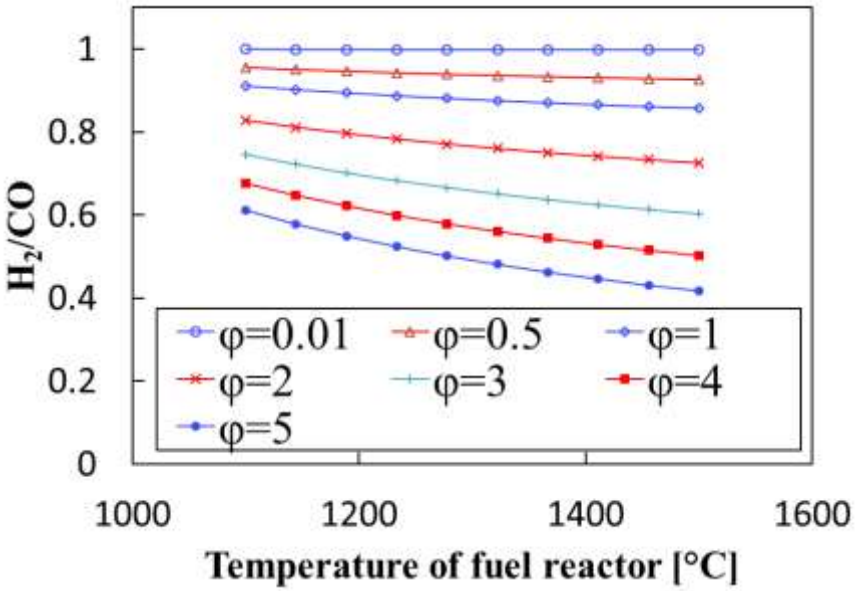

Fig. 9. The influence of temperature on the syngas quality for a range of values of ϕ.

6.4.Influence of temperature on the syngas quality for different ψ

Figure 10 presents the predicted influence of operating temperature on the syngas quality for different values of ψ. As shown, with an increase in ψ, the syngas quality increases. For example, with an increase in ψ from 0.1 to 1, the syngas quality increases from 0.78 to 1. This is because the production of H_2 depends on the availability of steam. In contrast to H_2, production of CO_2 increases weakly with an increase in ψ, since steam promotes the water-gas shift reaction to convert more CO to CO_2. In addition, an increase in temperature was found to decrease the syngas quality slightly because an increase in temperature favours the production of CO. For $0.1<\psi<1$, the variation of syngas quality with temperature is insignificant and with an increase in ψ, the syngas quality increases slightly. However, for further increases in ψ beyond unity, the syngas quality increases significantly. In addition, the role of temperature on the decrease of syngas quality is stronger. Therefore, the condition of $H_2/CO > 2$ can be achieved for $0.01<\varphi<0.1$ and $\psi>1$.

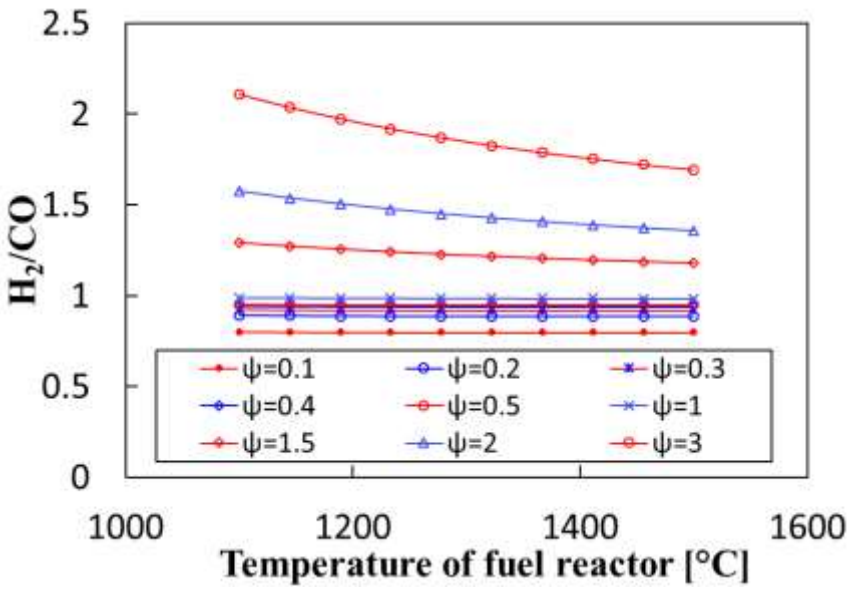

Fig. 10. Influence of temperature on the syngas quality for a range of values of ψ at φ=0.06. The stoichiometric value for ψ is 1 (blue line with "×" marker).

6.5.Influence of partial pressure of oxygen on syngas quality

The influence of partial pressure of oxygen on the syngas quality produced in the fuel reactor is presented in Figure 11. As shown, the mole fractions of the CO and H_2 decrease with an increase in partial pressure of oxygen. Syngas quality is also increased by an increase in partial pressure of oxygen, which is due to the decrease in CO production. However, a minimum partial pressure of oxygen is required to avoid solidification of CuO and Cu_2O, that is, to avoid two-phase operation (see Fig. 1), with an anticipated system failure. Given the need for a buffer to avoid solidification, it can be seen that it is difficult to achieve a syngas quality of higher than 0.84, which is well below the target value of 2.

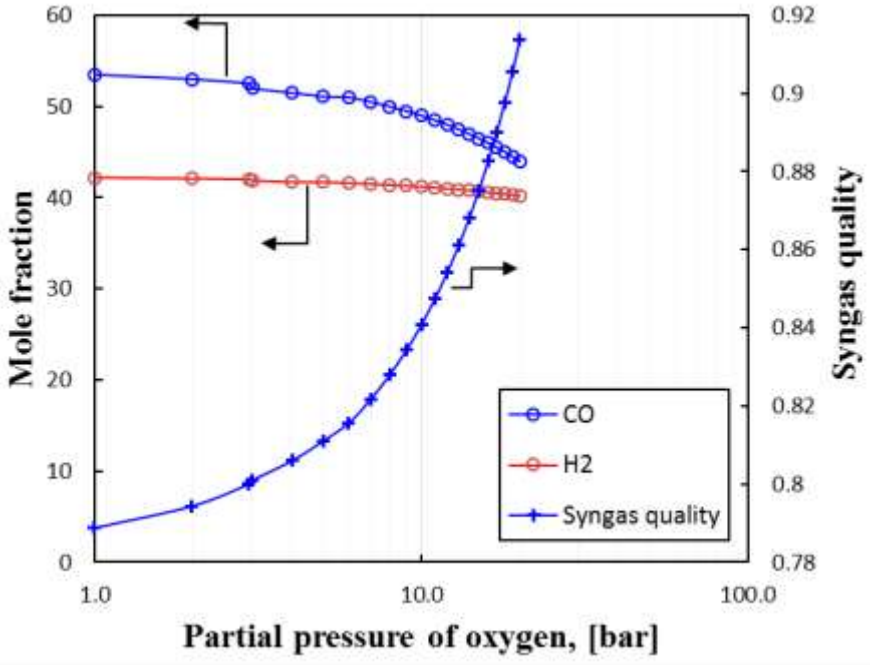

Fig.11. Dependence of production of H_2 and CO, together with the corresponding syngas quality, on partial pressure of oxygen in the fuel reactor.

6.6.Oxidation reactor

Figure 12 presents the dependence of the mole fraction of CuO and Cu_2O on λ_O at 1350°C. As can be seen, an increase in λ_O results in the increase in the number of moles of CuO, while mole fraction of Cu_2O decreases. Since CuO is the target product, a high value of λ_O is desirable. For $\lambda_O = 5$, the mole fraction of CuO reaches 0.89. While that of Cu_2O is minimised. For $\lambda_O \geq 8$, the mole fractions Cu_2O and CuO are constant. For these conditions, the ratio of regeneration, i.e. the value of CuO/Cu_2O= 17:3.

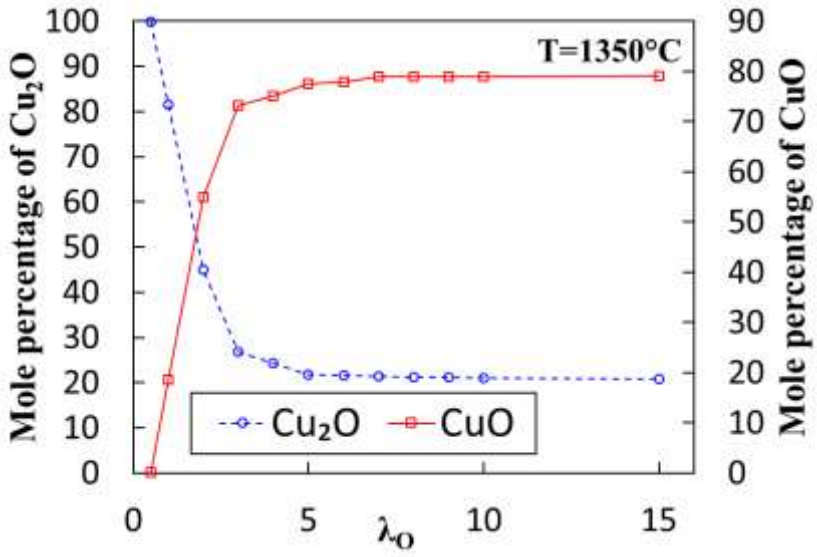

Fig. 12. Dependence on λ_O of the number of moles of CuO and Cu_2O in the product from the oxidation reactor.

6.7.Graphite conversion

Figure 13 presents the dependence of the calculated conversion of graphite on φ for three different operating temperatures. Three regimes can be seen, regime I, ($0<\varphi<8$) corresponds to LCLG mode, regime II, ($8<\varphi<13$) corresponds to the mode of mixed combustion and gasification, while regime III ($13<\varphi<20$) corresponds to complete oxidation of graphite (the LCLC regime). As can be seen, carbon conversion increases with an increase in ϕ, although the rate of increase depends on the partial pressure of oxygen available in the system. For the LCLG mode, carbon conversion is as high as 0.89 (regardless of the optimization of other operating parameters), while carbon conversion is unity in the LCLC mode. These results show that the slope of change for carbon conversion becomes zero for a conversion of 1. However, for the mixed combustion/gasification regime, the slope is higher for the gasification region, meaning that graphite is fully converted in the LCLC regime. This is because the combustion is complete. In addition, an increase in temperature was found to also increase the carbon conversion process slightly.

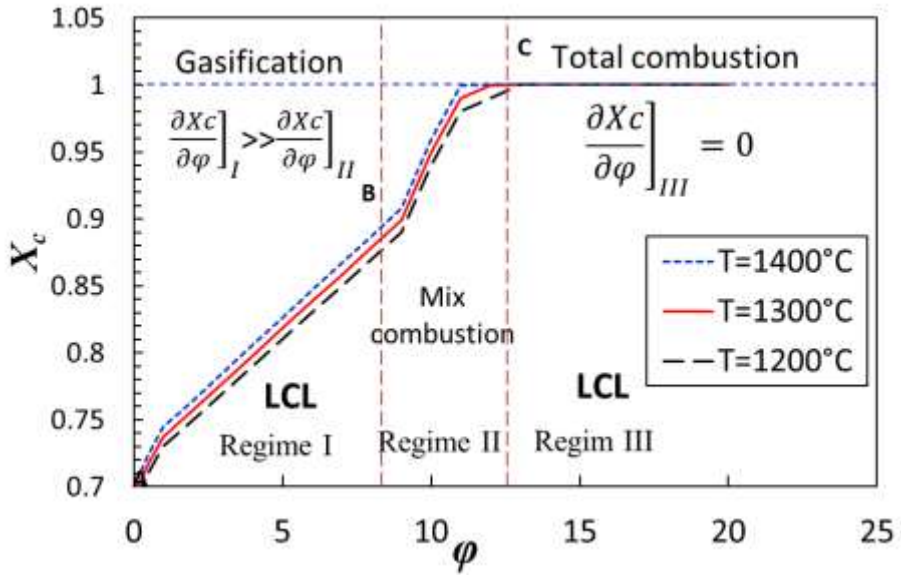

Fig. 13. Dependence of fuel conversion on φ for different operating temperatures of the gasifier for the regimes of liquid chemical looping gasification and combustion.

Figure 14 presents the calculated graphite conversion with the LCLG model in comparison with those reported in the literature for other gasification process [63-67] at the same temperature. As can be seen, the obtained results agree with previously reported data to within an absolute average difference of 6.5%. The comparison was performed at temperatures ranging from 1000°C and 1300°C to show that the fuel conversion for the gasification with molten metal oxides is effectively the same as those reported for other gasification processes and techniques. For example, the difference between the present and previous results are 3.1%, 5.1%, 6.5% and 2.6% for Siriwardane et al. [65], Dennis et al. [67], Li et al. [63] and Yu et al. [64], respectively.

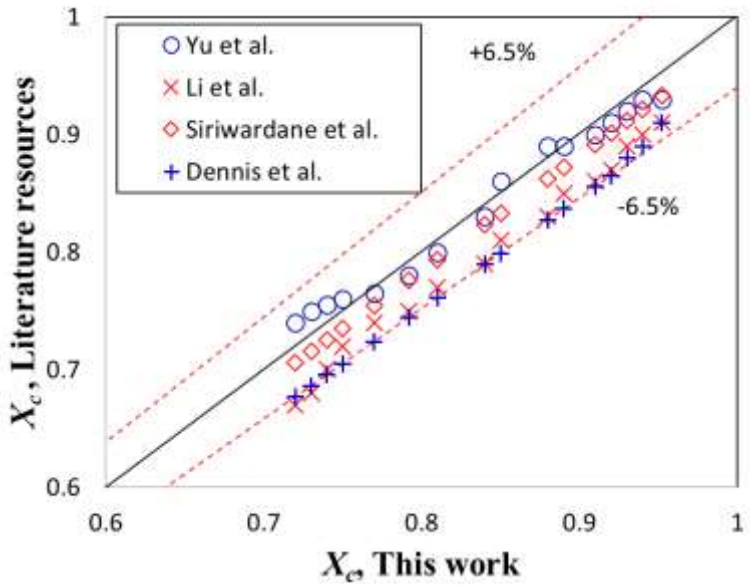

Fig. 14. A comparison between the conversion extent calculated in this study for LCLG and those of reported previously for conventional gasification at 1300°C.

6.8.Exergy analysis

Figure 15 presents the dependence of fraction of exergy in the syngas product and the hot vitiated air on the circulation ratio. As can be seen, an increase in the syngas quality is associated with an increase in the exergy transported by the syngas. This means that decreasing the circulation ratio causes the system to operate in the liquid chemical looping gasification mode. Conversely, an increase in φ promotes a shift toward the chemical looping combustion mode and an increase in the share of the exergy that is removed by the hot gases.

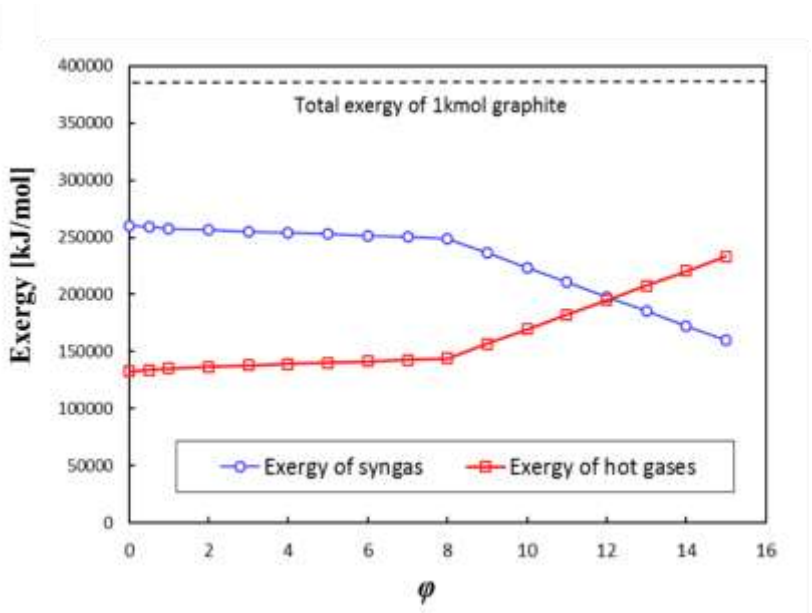

Fig. 15. Dependence on φ of exergy in syngas and hot gases (CO_2+H_2O+vitiated air) at T=1350°C.

Figure 16 presents the dependence of exergy fraction of the syngas and hot gases from the air reactor on φ for T=1350°C. As can be seen, for $\varphi \leq 8$, about 67% of total exergy of fuel is carried by the syngas product, while the remainder is carried by the hot gases the air reactor. However, with an increase in the circulation ratio, the exergy fraction of the syngas decreases. For φ=12 the amount of exergy is distributed equally to the syngas and hot gases, while for higher values of circulation ratio, the system moves into the chemical looping combustion regime, with majority of the exergy released to the hot gases. For example, at φ=15, 60% of exergy is partitioned to the hot gas and 40% to the syngas product.

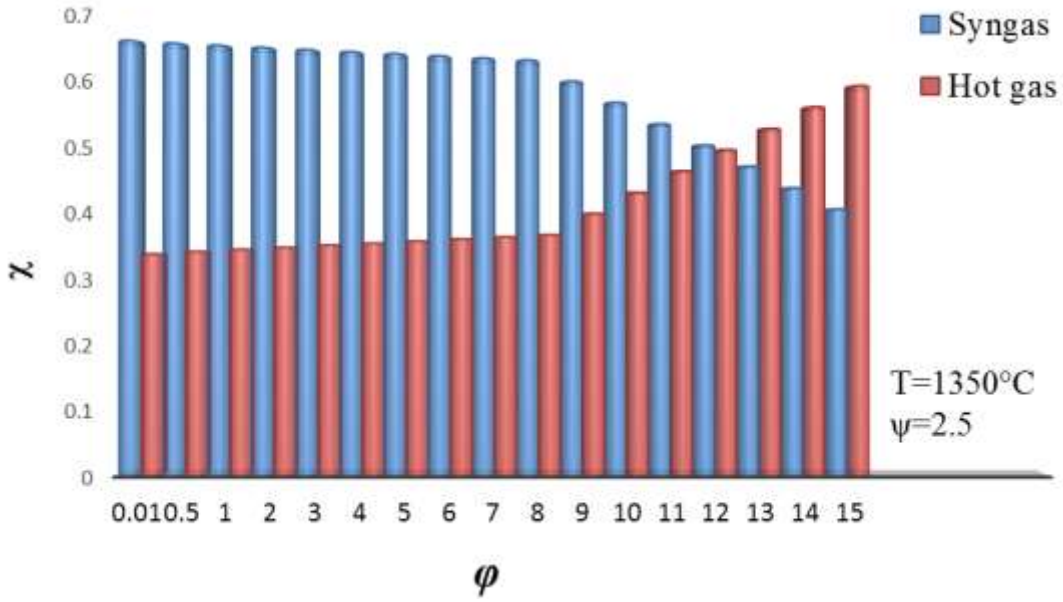

Fig. 16. Dependence on φ of exergy fraction of the syngas product at a temperature of 1350°C and for ψ=2.5 and for syngas product and hot gases (H_2O+CO_2+vitiated air).

7. Potential benefits and technical challenges

It is important to distinguish between the wider potential of the LCLG concept and the limitations of the system analysed here. The system has been analysed for CuO, in part because of the better availability of thermo-chemical and thermo-chemical data for copper than for other metals. The use of this metal, nevertheless introduces challenges associated with a high operating temperature and corrosiveness. However, the concept offers the potential to bypass some of the key challenges that have plagued chemical looping gasification with solid particles

provided that suitable metal/oxide combinations can be identified the possibility of identifying other metal oxides that may achieve comparable benefits at a lower temperature and reasonable pressures. It also offers the potential for hybridization with concentrated solar energy to drive the endothermic reactions.

The technical challenges associated with the use of CuO for LCLG are as follows:

1) A high operating temperature: To the best of our knowledge, no continuous flow reactor has been demonstrated for liquid metal oxides at high temperature and pressure. For copper, a reactor must sustain temperatures higher than 1000°C and a pressure of 10 bar.

2) Fluid circulation: A method is required to circulate the molten metal at high temperature. To the best of author's knowledge, no such system is commercially available.

3) Heat loss and solidification challenge: Although the process operates with an overall exothermal reaction, heat losses must kept low and managed carefully to avoid solidification. Furthermore, the temperature difference between operation and freezing point should be sufficiently great, which is not the case with copper.

4) Robust injection method: It is necessary to avoid local solidification near to the region where the gasifying agent and fuel are injected.

8. Conclusions

The analysis has demonstrated the thermodynamic potential of a new gasification system, in which a liquid metal oxide is employed as the gasification medium. This system offers significant potential benefits if the disadvantages associated with the use of the particular metal oxide chosen here (copper oxide) can be overcome, such as by identification of an alternative metal oxide with a lower operating temperature. The thermodynamic equilibrium analysis of the gasification of carbon using liquid copper oxide has revealed the following:

- Metal oxides (here copper oxide) are a suitable candidate for the gasification process in terms of heat and mass transfer, based on the Gibbs minimization method. From the Ellingham diagram, all potential gasification reactions are feasible, providing that the appropriate pressure and temperature are chosen.
- The gasification process via liquid copper oxide can be achieved isothermally with the same temperature in both reactors, although this requires them to be operated at different pressures. Furthermore, the process is thermally balanced, meaning that the

required heat for the gasification is supplied by the heat released from the oxidation of LOC in the air reactor.

- The pressure was found to have insignificant impact on the syngas production, while it is a controlling parameter of the physical state and stability of the liquid copper oxide. The ratio of LOC to fuel is another important parameter.

The LCLG proposed concept also offers potential to overcome the challenges related to the implementation of the solid oxygen carriers in CLG systems such as sintering, carbon deposition and agglomeration. However, to achieve this, technical challenges of high temperature operation, such as those identified in the discussion, need to be addressed. In addition, new experimental data are required to enable the better development and validation of models.

Nomenclature

A	constant
C_p	Specific molar heat capacity, kJ. $kmol^{-1}$.°C
G	Gibbs free energy, kJ
i	component
j	component
L	Lagrange multiplier
n	Mole fraction
N	Number of all component
P	Pressure, bar
R	Gas constant, J. $°C^{-1}$. mol^{-1}
T	Temperature, °C
x_o	Mole fraction of oxygen in liquid copper oxide

Greek letters

α	Constant, see equation 1
β	Constant, see equation 1
ζ	Constant, see equation 1
α	Activity coefficient
φ	Liquid oxygen carrier to fuel ratio
ψ	Steam to fuel ratio

γ	Carbon conversion
η	Thermal balance ratio
μ	Chemical potential
λ_O	Air to liquid oxygen carrier ratio

Acronyms

CLC	Chemical Looping Combustion
CLG	Chemical Looping Gasification
CLR	Chemical Looping Reforming
LHV	Lower heating value, kJ. $kmol^{-1}$
LOC	Liquid Oxygen Carrier
Gasif.	Gasification
LCLC	Liquid Chemical Looping Combustion
LCLG	Liquid Chemical Looping Gasification
Sens.	Sensible heat, kJ

Acknowledgements

Authors of this work gratefully acknowledge Australian Research Council (ARC) for the financial support through grant DP150102230. The first author of this work acknowledges "Australian Government Research Training Program Scholarship" for the financial supports. Also, Centre for energy technology is gratefully acknowledged for its financial and scientific supports.

References

[1] Wang P, Means N, Shekhawat D, Berry D, Massoudi M. Chemical-Looping Combustion and Gasification of Coals and Oxygen Carrier Development: A Brief Review. Energies. 2015;8:10605-35.
[2] Devi L, Ptasinski KJ, Janssen FJ. A review of the primary measures for tar elimination in biomass gasification processes. Biomass and bioenergy. 2003;24:125-40.
[3] Kirubakaran V, Sivaramakrishnan V, Nalini R, Sekar T, Premalatha M, Subramanian P. A review on gasification of biomass. Renewable and Sustainable Energy Reviews. 2009;13:179-86.
[4] Mehdi Jafarian MA, Graham Nathan. Thermodynamic potential of molten copper oxide for high temperature solar energy storage and oxygen production. Applied Energy. 2017;Under-review.
[5] Adanez J, Abad A, Garcia-Labiano F, Gayan P, Luis F. Progress in chemical-looping combustion and reforming technologies. Progress in Energy and Combustion Science. 2012;38:215-82.
[6] Jafarian M, Arjomandi M, Nathan GJ. A hybrid solar and chemical looping combustion system for solar thermal energy storage. Applied Energy. 2013;103:671-8.

[7] Jafarian M, Arjomandi M, Nathan GJ. A hybrid solar chemical looping combustion system with a high solar share. Applied Energy. 2014;126:69-77.
[8] Jafarian M, Arjomandi M, Nathan GJ. The energetic performance of a novel hybrid solar thermal & chemical looping combustion plant. Applied Energy. 2014;132:74-85.
[9] Tanner J, Bhattacharya S. Kinetics of CO 2 and steam gasification of Victorian brown coal chars. Chemical Engineering Journal. 2016;285:331-40.
[10] Patra TK, Sheth PN. Biomass gasification models for downdraft gasifier: A state-of-the-art review. Renewable and Sustainable Energy Reviews. 2015;50:583-93.
[11] Chan FL, Tanksale A. Review of recent developments in Ni-based catalysts for biomass gasification. Renewable and Sustainable Energy Reviews. 2014;38:428-38.
[12] Ge H, Guo W, Shen L, Song T, Xiao J. Biomass gasification using chemical looping in a 25kW th reactor with natural hematite as oxygen carrier. Chemical Engineering Journal. 2016;286:174-83.
[13] Adánez J, Gayán P, Celaya J, de Diego LF, García-Labiano F, Abad A. Chemical looping combustion in a 10 kWth prototype using a CuO/Al2O3 oxygen carrier: Effect of operating conditions on methane combustion. Industrial & Engineering Chemistry Research. 2006;45:6075-80.
[14] Li F, Kim HR, Sridhar D, Wang F, Zeng L, Chen J, et al. Syngas chemical looping gasification process: oxygen carrier particle selection and performance. Energy & Fuels. 2009;23:4182-9.
[15] Liao C, Wu C, Yan Y. The characteristics of inorganic elements in ashes from a 1 MW CFB biomass gasification power generation plant. Fuel processing technology. 2007;88:149-56.
[16] Fan L, Li F, Ramkumar S. Utilization of chemical looping strategy in coal gasification processes. Particuology. 2008;6:131-42.
[17] Acharya B, Dutta A, Basu P. Chemical-looping gasification of biomass for hydrogen-enriched gas production with in-process carbon dioxide capture. Energy & Fuels. 2009;23:5077-83.
[18] Anheden M, Svedberg G. Exergy analysis of chemical-looping combustion systems. Energy conversion and management. 1998;39:1967-80.
[19] Zevenhoven-Onderwater M, Backman R, Skrifvars B-J, Hupa M. The ash chemistry in fluidised bed gasification of biomass fuels. Part I: predicting the chemistry of melting ashes and ash–bed material interaction. Fuel. 2001;80:1489-502.
[20] Florin N. Calcium looping technologies for gasification and reforming. Calcium and Chemical Looping Technology for Power Generation and Carbon Dioxide (CO2) Capture. 2015.
[21] Li F, Zeng L, Velazquez-Vargas LG, Yoscovits Z, Fan LS. Syngas chemical looping gasification process: Bench-scale studies and reactor simulations. AIChE journal. 2010;56:2186-99.
[22] Fan L-S. Chemical looping systems for fossil energy conversions: John Wiley & Sons; 2011.
[23] Zafar Q, Mattisson T, Gevert B. Integrated hydrogen and power production with CO2 capture using chemical-looping reforming redox reactivity of particles of CuO, Mn2O3, NiO, and Fe2O3 using SiO2 as a support. Industrial & engineering chemistry research. 2005;44:3485-96.
[24] Tong A, Bayham S, Kathe MV, Zeng L, Luo S, Fan L-S. Iron-based syngas chemical looping process and coal-direct chemical looping process development at Ohio State University. Applied Energy. 2014;113:1836-45.
[25] Anthony EJ. Solid looping cycles: a new technology for coal conversion. Industrial & Engineering Chemistry Research. 2008;47:1747-54.
[26] Chen W-H, Lin M-R, Leu T-S, Du S-W. An evaluation of hydrogen production from the perspective of using blast furnace gas and coke oven gas as feedstocks. international journal of hydrogen energy. 2011;36:11727-37.
[27] Suopajärvi H, Pongrácz E, Fabritius T. The potential of using biomass-based reducing agents in the blast furnace: A review of thermochemical conversion technologies and assessments related to sustainability. Renewable and Sustainable Energy Reviews. 2013;25:511-28.
[28] Bafghi MS, Ito Y, Yamada S, Sano M. Effect of slag composition on the kinetics of the reduction of iron oxide in molten slag by graphite. ISIJ international. 1992;32:1280-6.
[29] Zhao Y, Sun S, Tian H, Qian J, Su F, Ling F. Characteristics of rice husk gasification in an entrained flow reactor. Bioresource technology. 2009;100:6040-4.

[30] Zhou J, Chen Q, Zhao H, Cao X, Mei Q, Luo Z, et al. Biomass–oxygen gasification in a high-temperature entrained-flow gasifier. Biotechnology advances. 2009;27:606-11.
[31] Ponzio A. Thermally homogenous gasification of biomass/coal/waste for medium or high calorific value syngas production: KTH; 2008.
[32] Liu J, Yu Q, Peng J, Hu X, Duan W. Thermal energy recovery from high-temperature blast furnace slag particles. International Communications in Heat and Mass Transfer. 2015;69:23-8.
[33] Barati M, Esfahani S, Utigard T. Energy recovery from high temperature slags. Energy. 2011;36:5440-9.
[34] Duan W, Yu Q, Xie H, Qin Q, Zuo Z. Thermodynamic analysis of hydrogen-rich gas generation from coal/steam gasification using blast furnace slag as heat carrier. international journal of hydrogen energy. 2014;39:11611-9.
[35] Duan W, Yu Q, Xie H, Liu J, Wang K, Qin Q, et al. Thermodynamic analysis of synergistic coal gasification using blast furnace slag as heat carrier. International Journal of Hydrogen Energy. 2015.
[36] Rezaei H, Gupta R, Bryant G, Hart J, Liu G, Bailey C, et al. Thermal conductivity of coal ash and slags and models used. Fuel. 2000;79:1697-710.
[37] Sinfelt JH, Carter J, Yates D. Catalytic hydrogenolysis and dehydrogenation over copper-nickel alloys. Journal of Catalysis. 1972;24:283-96.
[38] Rudloff WK, Freeman ES. Catalytic effect of metal oxides on thermal decomposition reactions. II. Catalytic effect of metal oxides on the thermal decomposition of potassium chlorate and potassium perchlorate as detected by thermal analysis methods. The Journal of Physical Chemistry. 1970;74:3317-24.
[39] Harlé V, Vrinat M, Scharff J, Durand B, Deloume J. Catalysis assisted characterizations of nanosized TiO 2–Al 2 O 3 mixtures obtained in molten alkali metal nitrates: Effect of the metal precursor. Applied Catalysis A: General. 2000;196:261-9.
[40] Barin I. Thermochemical Data of Pure Substances, Thermochemical Data of Pure Substances: Wiley-VCH; 1997.
[41] Shishin D, Decterov SA. Critical assessment and thermodynamic modeling of the Cu–O and Cu–O–S systems. Calphad. 2012;38:59-70.
[42] Kosenko A, Emel'chenko G. Equilibrium phase relationships in the system Cu-O under high oxygen pressure. Journal of phase equilibria. 2001;22:12-9.
[43] McKee D. The copper-catalyzed oxidation of graphite. Carbon. 1970;8:131IN3137-136IN8139.
[44] Jernigan G, Somorjai G. Carbon monoxide oxidation over three different oxidation states of copper: metallic copper, copper (I) oxide, and copper (II) oxide-a surface science and kinetic study. Journal of Catalysis. 1994;147:567-77.
[45] Forghani A, Jafarian M, Pendleton P, Lewis D. Mathematical modelling of a hydrocracking reactor for triglyceride conversion to biofuel: model establishment and validation. International Journal of Energy Research. 2014;38:1624-34.
[46] Ding Y, Alpay E. Adsorption-enhanced steam–methane reforming. Chemical Engineering Science. 2000;55:3929-40.
[47] Grenoble D, Estadt M, Ollis D. The chemistry and catalysis of the water gas shift reaction: 1. The kinetics over supported metal catalysts. Journal of Catalysis. 1981;67:90-102.
[48] Jafarian S, Haseli P, Karimi G. Performance analysis of a solid oxide fuel cell with reformed natural gas fuel. International Journal of Energy Research. 2010;34:946-61.
[49] Calo J, Perkins M. A heterogeneous surface model for the "steady-state" kinetics of the Boudouard reaction. Carbon. 1987;25:395-407.
[50] Newsome DS. The water-gas shift reaction. Catalysis Reviews Science and Engineering. 1980;21:275-318.
[51] Sarafraz M, Hormozi F. Scale formation and subcooled flow boiling heat transfer of CuO–water nanofluid inside the vertical annulus. Experimental Thermal and Fluid Science. 2014;52:205-14.

[52] Sarafraz M, Hormozi F. Convective boiling and particulate fouling of stabilized CuO-ethylene glycol nanofluids inside the annular heat exchanger. International Communications in Heat and Mass Transfer. 2014;53:116-23.
[53] Sarafraz M, Hormozi F. Nucleate pool boiling heat transfer characteristics of dilute Al 2 O 3–ethyleneglycol nanofluids. International Communications in Heat and Mass Transfer. 2014;58:96-104.
[54] Sarafraz M, Kiani T, Hormozi F. Critical heat flux and pool boiling heat transfer analysis of synthesized zirconia aqueous nano-fluids. International Communications in Heat and Mass Transfer. 2016;70:75-83.
[55] Sarafraz MM. Nucleate pool boiling of aqueous solution of citric acid on a smoothed horizontal cylinder. Heat and Mass Transfer. 2012;48:611-9.
[56] Sarafraz M, Hormozi F, Peyghambarzadeh S. Pool boiling heat transfer to aqueous alumina nano-fluids on the plain and concentric circular micro-structured (CCM) surfaces. Experimental Thermal and Fluid Science. 2016;72:125-39.
[57] Sarafraz M, Hormozi F, Silakhori M, Peyghambarzadeh S. On the fouling formation of functionalized and non-functionalized carbon nanotube nano-fluids under pool boiling condition. Applied Thermal Engineering. 2016;95:433-44.
[58] Coats HM. Ash-separator. Google Patents; 1907.
[59] John Y. Multiple element vortical whirl ash separator. Google Patents; 1952.
[60] Wen C-Y, Lee ES. Coal conversion technology. NASA STI/Recon Technical Report A. 1979;79:53776.
[61] Duan W, Yu Q, Xie H, Liu J, Wang K, Qin Q, et al. Thermodynamic analysis of synergistic coal gasification using blast furnace slag as heat carrier. International Journal of Hydrogen Energy. 2016;41:1502-12.
[62] Yun Y, Chung SW, Yoo YD. Syngas quality in gasification of high moisture municipal solid wastes. Prepr Pap-Am Chem Soc, Div Fuel Chem. 2003;48:823.
[63] Li P, Lei W, Wu B, Yu Q. CO 2 gasification rate analysis of coal in molten blast furnace slag—For heat recovery from molten slag by using a chemical reaction. International Journal of Hydrogen Energy. 2015;40:1607-15.
[64] Duan W, Yu Q, Liu J, Hou L, Xie H, Wang K, et al. Characterizations of the hot blast furnace slag on coal gasification reaction. Applied Thermal Engineering. 2016.
[65] Siriwardane R, Riley J, Tian H, Richards G. Chemical looping coal gasification with calcium ferrite and barium ferrite via solid–solid reactions. Applied Energy. 2016;165:952-66.
[66] Boyd RM, Fischer DD, Humphrey AE, King SB, Whitman DL. Method for in situ coal gasification operations. Google Patents; 1981.
[67] Dennis JS, Scott SA. In situ gasification of a lignite coal and CO 2 separation using chemical looping with a Cu-based oxygen carrier. Fuel. 2010;89:1623-40.